Springer

KSME

Journal of Mechanical Science and Technology 33 (2) (2019) 773~782
www.springerlink.com/content/1738-494x(Print)/1976-3824(Online)
DOI 10.1007/s12206-019-0132-5

Thermal analysis for the large precision EDM machine tool considering the spark energy during long-time processing †

Zhaoxi Zhao[1,2], Yukui Wang[1,2], Zhenlong Wang[1,2,*] and Jianyong Liu[3]

[1]*Key Laboratory of Micro-systems and Micro-structures Manufacturing of Ministry of Education, Harbin Institute of Technology, Harbin, 150001, China*
[2]*School of Mechatronics Engineering, Harbin Institute of Technology, Harbin, 150001, China*
[3]*Beijing Institute of Electromachining, Beijing, 100000, China*

(Manuscript Received March 11, 2018; Revised September 7, 2018; Accepted September 18, 2018)

Abstract

Thermal error is a major factor influencing the accuracy of large precision electrical discharge machining (EDM) machine tools, especially when processing continuously for a long time. In this paper, a novel thermal analysis model was set up to identify the static and dynamic thermal behaviour of the large EDM machine tool. The thermal effect of multiple spark discharges is considered. An equivalent heat flux method was proposed to model the intermittent heat flux for the first time. Both the steady and transient analyses were applied to investigate the thermal equilibrium time of critical points. It is found that when the study point is far away from the heat source, the longer thermal equilibrium time is needed. And the thermal equilibrium time of the machine tool was also estimated. Verification experiment has been performed, indicating the simulation accuracy of 87 % on the temperature rise of the electrode. Moreover, on the displacement of the spindle, the simulated result matched with the experimental result in Z direction error of 7 %. Finally, suggestions for reducing the thermal deformation were proposed to further improve the machining accuracy of large EDM machine tools.

Keywords: Large precision EDM machine tools; Thermal characteristics; Spark energy; Finite element analysis

1. Introduction

Thermal error, widely studied in the cutting machine tools [1, 2], is usually ignored in the small EDM machines and has not received much attentions in the large ones. However, the thermal error can seriously influence the accuracy of the large precision EDM machine tools in practice, especially when processing continuously for a long time. However, investigations of thermal characteristics of EDM machine tools have almost not been addressed yet, which is due to the lower power of shaft motor and less heat generation when comparing with metal cutting machine tools [3]. Nowadays, with the emergence of large monolithic parts in the aerospace industry [4] such as integral impellers and aeroturbine disks, EDM machine tools for manufacturing these parts are developing to be large scale. Moreover, high machining accuracy and long processing cycle (about 200 to 300 hours) of these parts put forward strict precision and reliability requirements to the machine tools [5].

For the thermal analysis based on EDM, many investigations have concentrated upon the thermal modelling of single discharge. Ahmed et al. presented a thermal analysis model of EDM and hybrid electrical discharge to compare their respective transient temperature distribution and the erosion efficiencies after a single-pulse discharge [6]. Zhao et al. investigated the thermo-physical properties of SiC through heat transfer analysis of a single discharge [7]. The aim of previous studies is to obtain the crater morphology and working surface temperature for studying the EDM mechanism and processing characteristics of materials. Furthermore, the thermal model is based on the assumption that the heat flux on the working surface is distributed as Gauss heat source [8, 9]. In fact, EDM is a consecutive pulse discharge process. Since the electrical phenomena of the plasma channel involving superposition, migration and abruption are of stochastic nature, the scientific insight into single pulse experiment field is insufficient [10]. For multiple discharges, K. P. Somashekar applied a numerical technique to predict the effect of spark ratio on the temperature distribution and thereby realized that temperature oscillation was obvious when spark ratio was more [11]. Varghese et al. have done simulations for multiple discharges (5 discharges) in order to get insight into accumulation of workpiece surface temperature [12]. Klocke et al. provided an inverse thermal method for estimating the energy distribution

*Corresponding author. Tel.: +86 13703640831, Fax.: +86 413485
E-mail address: wangzl@hit.edu.cn
† Recommended by Associate Editor Wonkyun Lee

of the electrode after a sustaining EDM process [13]. The above investigations on multiple discharges are based on a point heat source model of a single discharge whereby machined geometry, material removal, electrode wear and energy distribution can be worked out.

In fact, during an actual EDM operation, the processing time is generally on the order of hundreds of hours, and the accumulation of generated heat may have a great impact on the accuracy of large precision EDM machine tools. Hence, the single discharge model and several discharges model controlled by limited time steps in simulations could not provide insight into the long-time thermal effect on machine tools. Furthermore, different from small and medium-sized EDM machine tools, the longer processing time and larger machining area result in more heat generation at structural parts. Hence, the research on thermal characteristics of large precision EDM machine tools is indispensable. Since thermal test subjects to the constraints for complexity, cost and time consumption [14], finite element analysis (FEA) has been widely used as a valid tool in predicting thermal behavior of machine tool especially for long-time processing in some cases [15].

In this paper, a novel thermal analysis model is set up to get the thermal behavior of critical parts on the large precision EDM machine tool using FEA method. In the meanwhile, the concept of equivalent heat flux is proposed which is capable of simulating the superposition of successive discharge. Both the steady and transient analyses are applied to investigate the thermal equilibrium time of critical points. And the thermal equilibrium time of the machine tool is also estimated. Then, verification experiment has been performed to assess the accuracy of simulation model and good agreement is observed between the experiment measurements and simulation results.

2. Numerical modelling setup of the machine tool

2.1 The instruction for the machine tool

Based on the above, the A2190 large precision six-axis linkage NC die-sinking EDM machine tool is selected as the research object, which is suitable for manufacturing large aeroturbine disks, aero-engine impeller nozzle cascade and other aerospace parts. The simplified geometry model of the machine is shown in Fig. 1(a). The workpiece presented in this article is an integral blisk whose diameter is 600 mm with a hub and 30 blades along the profile direction. As shown in Fig. 1(b), the reserve copy process is accomplished by the integral electrode. The radial direction of the blisk is used as the feed direction during a single blade manufacturing. After that, the electrode driven by C-axis will be moved a given angle (12°) along the radial direction to copy the next blade. It takes about 300 hours to finish the rough machining of a turbine disk.

2.2 Modelling of FEA and heat transfer process

The modelling process consists of the FEA model of the

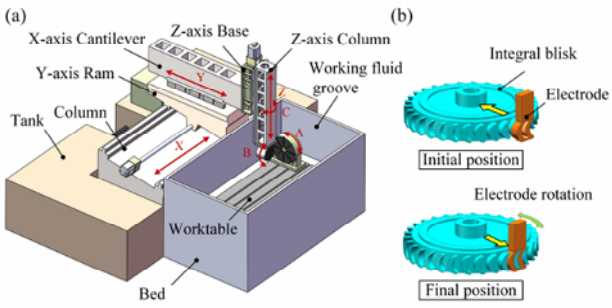

Fig. 1. The model of the EDM machine tool; (a) The simplified geometry model of the large EDM machine tool; (b) the erosion path of the electrode.

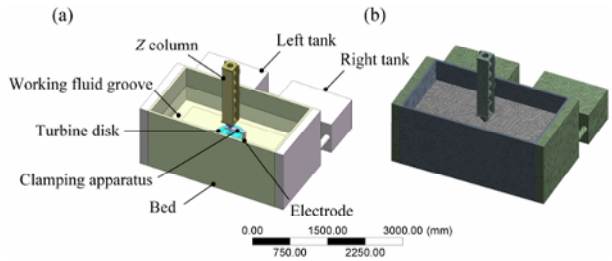

Fig. 2. Establishment of physical model in simulation; (a) 3D geometry model; (b) finite element model.

structural components and process-related heat transfer model. In order to guarantee the validity of modeling, the most essential components of the machine should be modeled and other components are suspended from the consideration. With respect to characteristics including holes, small stairs, chamfers, and bolt holes are further simplified. As shown in Fig. 2(a), the structure is equipped with bed, Z column, working liquid groove, left and right tanks, electrode, clamping apparatus and turbine disc. As shown in Fig. 2(b), this model has been divided into 2084914 elements in ANSYS mesh module. Moreover, the simulation verification of grid consistency has been completed before this.

In the process of EDM, the Joule heating effect is the main source of thermal energy increasing the discharge channel temperature and melting both electrodes. The above-acknowledged Gauss distribution is employed as the heat source model of the plasma expansion release in the present study. The $q(r)$ represents the heat flux density at the distance of r from the central point of the discharge (W/m^2). The Gauss heat source model is defined by Eq. (1) [16].

$$q(r)=\frac{3\eta UI}{\pi r_h^2}\exp\left(-\frac{3r^2}{r_h^2}\right) \tag{1}$$

where η is the energy distribution coefficient, U is the sustaining voltage of spark discharge (V), I is the peak current (A), r is the distance from the central point of discharge (m) and r_h is the spark radius (m).

Spark radius is critical in the thermal modeling of EDM

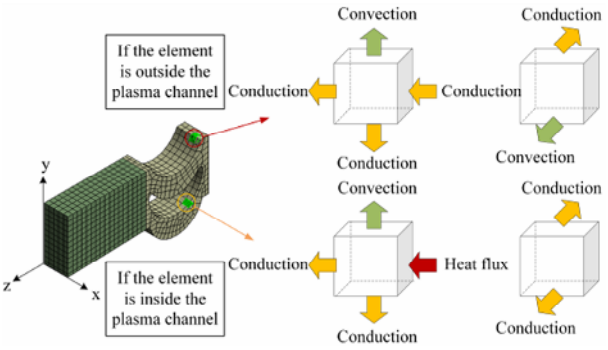

Fig. 3. Example of hexahedral element and its boundary conditions.

process. Different approaches have been proposed to estimate spark radius in the literature. Singh et al. have derived a semi-empirical equation given by discharge current and discharge on-time t_{on} [17].

$$r_h = 0.00204 I^{0.43} t_{on}^{0.44}. \tag{2}$$

With regard to multiple discharges superimposed model, the boundary conditions of the element are determined by the location and the time-varying heat source in each time step. In this study, the thermal boundary conditions of elements consists of the heat flux due to EDM sparks, heat flow rate by conduction and heat flow rate by convection with air or working fluid. Heat accumulation rate of each element may be a comprehensive effect as a combination of one, two or three of them, depending on if it is directly affected by the heat input or not [18]. Fig. 3 shows the illustration of the heat transfer that flows through the elements on the electrode surface.

The element inside the plasma channel is considered as an example. The heat flux as a boundary condition flows into the right surface. Meanwhile, the surfaces contacting the work fluid is thermal convection, and heat flow from the other surfaces is in the form of heat conduction. The differential equation of heat flux into the element is

$$\dot{Q}_{right} = q dydz \tag{3}$$

where q is the heat inflow of the element, dy and dz is the dimensions of the elemental. Supposing that h is the convection coefficient of working fluid, the quantity of heat flowing out of the element in the form of heat convection is derived from:

$$\dot{Q}_{up} = h\left(T_{x,y,z,m} - T_f\right) dxdz \tag{4}$$

where $T_{x,y,z,m}$ is the temperature of the element in X,Y,Z coordinates in instant m (K) and T_f is the ambient temperature of air or working fluid (K). The quantities of heat flowing out of the other element surfaces in the form of heat conduction are

$$\dot{Q}_{left} = -k \frac{\partial T}{\partial x}\bigg|_{left} dydz \tag{5}$$

$$\dot{Q}_{front} = -k \frac{\partial T}{\partial z}\bigg|_{right} dxdy \tag{6}$$

$$\dot{Q}_{down} = -k \frac{\partial T}{\partial y}\bigg|_{down} dxdz \tag{7}$$

$$\dot{Q}_{back} = -k \frac{\partial T}{\partial z}\bigg|_{back} dxdy \tag{8}$$

where k is the thermal conductivity (W/(m·K)). The accumulated heat inside an element is expressed as

$$\dot{Q}_{accumulated} = \rho C_p dxdydz \cdot \frac{\partial T}{\partial t} \tag{9}$$

where ρ is mass density (kg/m^2) and C_p is the specific heat (J/(kg·K)). Then the heat balance equation of the element inside the plasma channel is

$$\begin{aligned} &qdydz - h\left(T_{x,y,z,m} - T_f\right) dxdz - k \frac{\partial T}{\partial x}\bigg|_{left} dydz - k \frac{\partial T}{\partial z}\bigg|_{front} dxdy \\ &- k \frac{\partial T}{\partial y}\bigg|_{down} dxdz - k \frac{\partial T}{\partial z}\bigg|_{back} dxdy = \rho C_p dxdydz \cdot \frac{\partial T}{\partial t}. \end{aligned} \tag{10}$$

Analogously, the heat balance equation of the element outside the plasma channel is

$$\begin{aligned} &k \frac{\partial T}{\partial x}\bigg|_{right} dydz - h\left(T_{x,y,z,m} - T_f\right) dxdz - h\left(T_{x,y,z,m} - T_f\right) dxdy \\ &- k \frac{\partial T}{\partial x}\bigg|_{left} dydz - k \frac{\partial T}{\partial y}\bigg|_{down} dxdz - k \frac{\partial T}{\partial z}\bigg|_{back} dxdy = \rho C_p dxdydz \cdot \frac{\partial T}{\partial t}. \end{aligned} \tag{11}$$

3. The FEA process and simulation conditions setup

3.1 The FEA solution process

In this study, both the meshing and the simulation are carried out on Ansys15.0 Workbench coupling platform. The simulation process of this study is displayed in Fig. 4. At the beginning, the steady state fluid analysis is implemented through the fluent module according to the boundary condition of fan pressure jump as the working fluid pump flow. The inputs of the thermal analysis include the heat flux on the machining areas and the convective coefficient and free stream temperature. The temperature fields of the electrode and workpiece, working fluid, Z column, worktable and bed are calculated. Furthermore, the maximal temperature rises of the key points are as reference for the transient analysis. The thermal equilibrium times of working fluid, electrode and workpiece, Z column and worktable are performed through transient analysis. Then the results of the thermal analysis are

Table 1. Thermo-physical properties of TC4.

Properties	TC4				
Mass density (kg/m^2)	4850				
Specific heat (J/(kg·K))	20 °C	100 °C	200 °C	300 °C	400 °C
	611	624	653	674	691
	500 °C	1000 °C	1500 °C	2500 °C	-
	703	1030	1850	1852	-
Thermal conductivity (W/(m·K))	20 °C	100 °C	200 °C	300 °C	400 °C
	6.8	7.4	8.7	9.8	10.3
	500 °C	1000 °C	1500 °C	2500 °C	-
	11.8	15.5	22.1	22.2	-

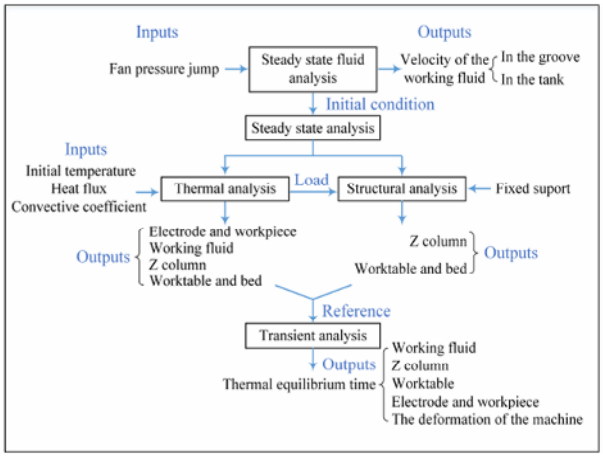

Fig. 4. The simulation process of this study.

served as the load to the latter structural analysis to achieve the deformation. The thermal equilibrium time of the deformation of the machine tool will be performed in this part.

3.2 The simulation conditions setup

During machining, the local temperature near discharge point rises from room temperature to the melting point of the material and then decreases to initial temperature within a few hundred microseconds. Thus, temperature-dependent thermo-physical properties must be considered precisely in the simulation process. The thermo-physical properties of TC4 applied in the current work are listed in Table 1. With regard to copper, the effect of temperature change on its thermophysical properties can be neglected, which is treated as a constant in this paper. The mass density (ρ), specific heat (Cp), and thermal conductivity (k) of copper is set as 8978 kg/m^2, 391 J/(kg·K) and 388 W/(m·K), respectively.

The applied process parameters and operating conditions are specified in Table 2. The workpiece material used in the simulation analysis is titanium alloy TC4 common for aerospace industry. Copper is selected as electrode material according to rough machining procedure. The percentages of the total heat conducted into the anode, cathode, and discharge

Table 2. Process parameters and operating conditions for simulation.

Parameters and conditions	Value
Workpiece material	TC4
Electrode material	Copper
Pulse width (μs)	500
Pulse interval (μs)	500
Gap voltage (V)	25
Peak current (A)	200
Initial temperature (K)	300
Working fluid pump flow (m^3/h)	3
Convective coefficient (W/m^2•K)	5
Working fluid	Kerosene
Working fluid circulation mode	Immersion processing

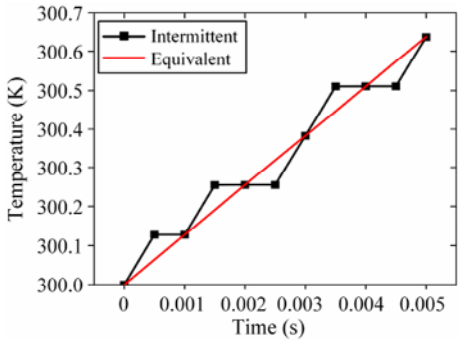

Fig. 5. Comparison of simulated temperature due to the intermittent and equivalent heat flux.

channels have no definite values, which are closely related to electrical parameters and non-electrical parameters [19, 20]. The workpiece and electrode are connected to the positive and negative polarity of the power, respectively. In this work, the cathode and anode energy distribution coefficients are 0.183 and 0.08, respectively, which have adopted the assumption by Kuriachen [16]. The initial temperature of simulation model is taken as 300 K.

3.3 The equivalent heat flux

The heat flux applied on the machining surface is derived from an increased temperature after a series of repetitive thermal load due to recurring electrical discharges. In consideration of reliable simulation results, the time step is expected to be equal to the common divisor between the pulse width t_{on} and the pulse interval t_{off}. In this work, both the pulse width and pulse interval is taken as 500 μs, so the time step Δt is taken as 500 μs in order to save computation cost. However, if the parallel computation is performed through a 16 cores computer, it takes one month for the processing time of 30 min. In the meanwhile, it has to simulate the EDM process for dozens of hours. Obviously, the efficiency of this method is very low, so that it is essential to seek an equivalent continuous heat source for simulation.

Accordingly, the heat flux of the whole machined surface termed as "equivalent heat flux" is calculated by integral. It is capable for simulating the thermal effect based on superposition of successive discharge. Besides, within a pulse duration, the effective machining area involved in a pulse width is 0.75 % of the total machining area and only 10 % of the total number of discharges produce normal discharge sparks [21]. The equivalent heat flux is expressed as Eq. (12).

$$q_{eq}(r)=\frac{3\cdot 0.75\%\cdot 10\%\eta UI}{2\pi r_h^2}\exp\left(-\frac{3r^2}{r_h^2}\right). \quad (12)$$

Substituting all the parameters into the equation, the average heat source of the two electrodes are calculated through the MATLAB software. As a result, the equivalent heat flux endured by the anode and the cathode surface is 3.3E+05 W/m^2 and 1.4E+05 W/m^2. To verify the accuracy of the equivalent calculation, comparison simulation between intermittent and equivalent heat flux is carried out. Fig. 5 displays the simulated temperature of the electrode at a depth of 2 mm from the machining surface within 10 pulse period. It is found that the result of equivalent heat flux is in good agreement with the intermittent one.

4. Results and discussion

4.1 Steady state thermal and deformation analysis

In this study, steady state velocity field is an important premise for thermal analysis. The convection effects of working fluid directly affects the dissipation of heat. Fig. 6 demonstrates the velocity field on the cross section of the working liquid groove and tanks. The working liquid flows from the right tank into the groove through the inlet and constantly flows out into the left tank through the outlet on the other side. And the waste oil flows into the right tank after being filtered in the left tank to complete a cycle process.

After fluid analysis, the thermal simulation on the machine structures has been implemented. The contour of temperature field of Y axis cross section is shown in Fig. 7(a). Because of the slight temperature rise of the working fluid in comparison with that of the machining surfaces, the range of the display temperature is adjusted to 300 K~350 K in order to give more information. It denotes the temperature of the working fluid around machining area and the upper surface of worktable is significantly improved. Some of the heat received from the machining surfaces is dissipated into the surrounding fluid. It leads to the overall increase of temperatures of the circulating working fluid and the surface of the worktable and bed, thus causing thermal deformation and degradation of the mechanical machining accuracy. According to the temperature field of the Z column in Fig. 7(b), the high temperature region is mainly concentrated on the lower end of the spindle head. In the light of natural convection, the relatively little temperature elevation occurs on the top. The maximal temperature rise of

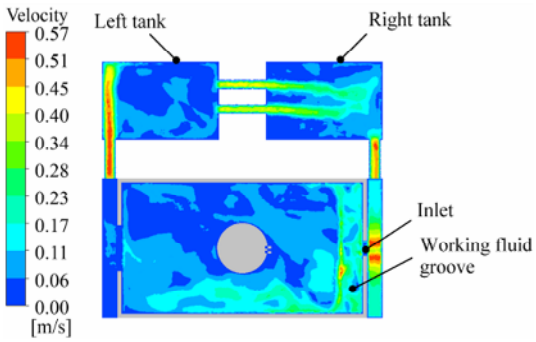

Fig. 6. Flow velocity contour of working fluid.

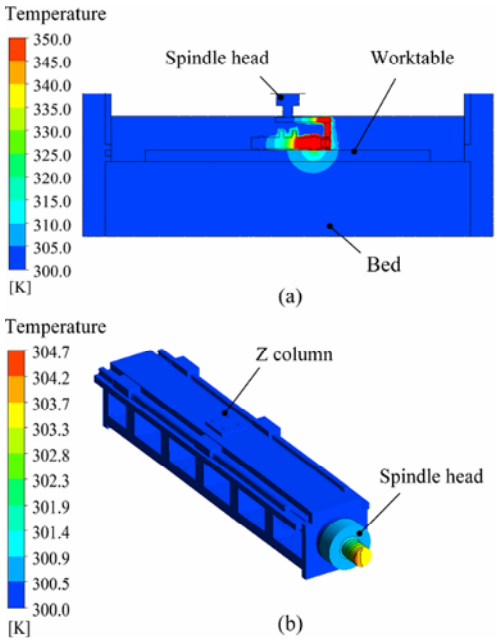

Fig. 7. Contour of temperature field distribution: (a) Y axis cross section; (b) Z column.

the Z column is about 4.7 K at the center of the lower end of the spindle head.

Neglecting the gravity, the coupling analysis of temperature and structure of Z column is figured out. The top surface of the nut seat and the bottom surface of the bed are set as fixed support as the boundary conditions for structural analysis of the whole machine tool. Fig. 8(a) indicates the maximal thermal deformation is located at the lower end of the spindle head coincident with that of the temperature field. Based on 3D thermal deformation plots of the Z column in Fig. 8(b), it can make several observations. First, since the machine tool components are basically symmetrical along X direction, Z column in X direction is evenly and symmetrically heated as a result. Secondly, the Z column along Y direction is not strictly symmetrical, and the maximal deformation in the Y direction is 5.7 μm.The deformations in the Y direction and X direction have little influence on the whole machine. Finally, the thermal deformation in the Z direction is 52 μm which is most dominant than the others. So the deformation of the Z column

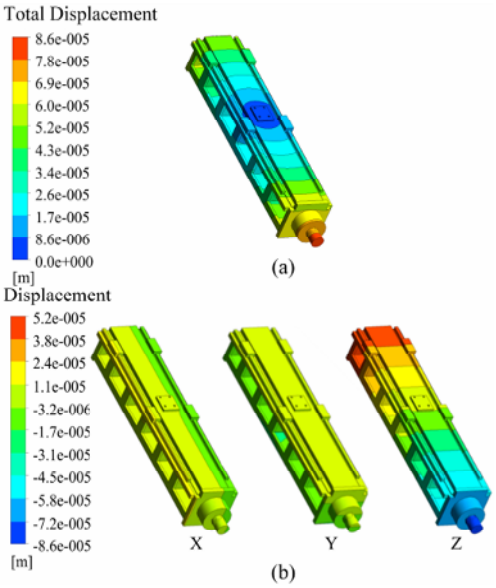

Fig. 8. The thermal deformation contour of the Z column: (a) Total deformation; (b) deformation in the X, Y and Z deformation.

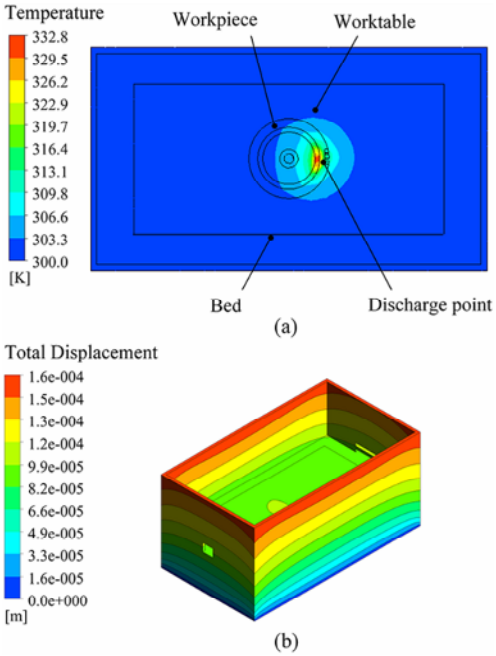

Fig. 9. The contour of worktable and bed: (a) The temperature contour; (b) the thermal deformation contour.

and the spindle head is mainly reflected in the axial elongation.

On the subject of the worktable and bed, the maximal temperature of the top surface is 332.8 K derived from the result. The coordinates of the point with the maximal temperature are (X:2021, Y:900, Z:600) which is in contact with the workpiece and the closest to the discharge point. Fig. 9 indicates the information about the temperature and deformation contour of worktable and bed separately. It manifests that the maximal deformation is at the top of the working fluid groove, with a deformation of 160 μm. The working fluid with high temperature gives rise to the elongation of worktable and bed, hence impacting upon the position of the workpiece relative to the electrode during a long time rough machining. The deformation of the worktable is the largest in the Z direction and the value is 64.2 μm.

4.2 Transient thermal and deformation analysis

Based on transient analysis, the thermal equilibrium time of the selected key points on the machine tool can be acquired severally after continuous processing. The X-coordinate of the curve indicates processing time and the Y-coordinate stands for temperature of the selected points. In a sense, the temperature data of the key points have been considered as the measured temperatures [22]. The selecting principle of the measuring point is to choose the points near the heat source, which can reflect a close interdependency with thermal deformation of the machine parts.

First, the average temperature rise curves of working fluid in the groove and the tank increasing with time are got. The maximal temperatures of the working fluid inside the groove and the tank are 304.85 K and 304.69 K in the steady state analysis, denoted by T_1 and T_2 respectively. Fig. 10(a) demonstrates that the average temperature of the working fluid in the groove rises rapidly within the first 50 hours during processing, and increases gradually with the circulation of the working fluid. The similar effects can also be observed for the average temperature rise of the working fluid in the tank (Fig. 10(b)). When the temperature rise increases to 95 % of the maximal temperature rise, it is treated as thermal equilibrium state. Accordingly, the thermal equilibrium time of the working fluid in the groove is about 60 hours, which is 5 hours shorter than that in the groove. This is because the tank is farther away from machining area.

Then, Figs. 10(c) and (d) indicate the temperature rise curves of the selected key points on the electrode and the workpiece. The selected point on the electrode is the vertex of the upper surface. And the selected point on the workpiece is on the circumference and the distance from the machining area is 200 mm. The maximal temperature of the points is expressed by T_3 and T_4. After 4 hours and 7 hours, the temperature rise of the points on the electrode and workpiece reach a stable value respectively. It is presents that the thermal equilibrium time of the electrode and the workpiece is very short. Similarly, the maximal temperature of the worktable is illustrated in Fig. 10(e). After 3 hours, the point tends to the thermal equilibrium state, which is much shorter relative to other parts on the machine tool as mentioned above.

The thermal equilibrium time of the machine tool is depends on the temperature rise of the worktable and the spindle head. The average temperature of the bottom of the spindle head T_6 increases with the time is illustrated in Fig. 10(f). The temperature has increased rapidly during the first 16 hours of the machining process and until about 56 hours it reaches

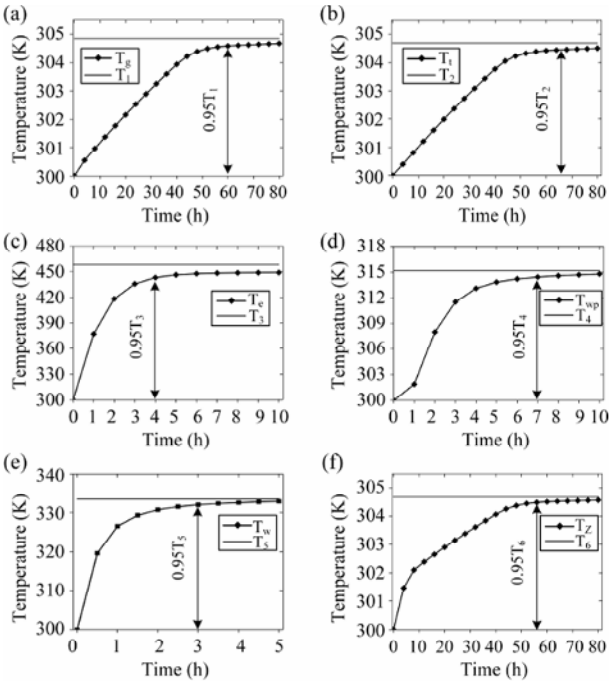

Fig. 10. The temperature rise of the selected key points on the machine tool: (a) The average temperature of the working fluid in the groove; (b) the average temperature of the working fluid in the tank; (c) the temperature of the electrode; (d) the temperature of the workpiece; (e) the maximum temperature of the worktable surface; (f) the average temperature of the bottom of the spindle head.

thermal equilibrium state.

Obtained from the above data, the thermal equilibrium times of the electrode and the workpiece are the shortest and the points on the worktable and the spindle head are second. The thermal equilibrium times of working fluid inside the groove and the tank are the longest as well. The thermal equilibrium time of each key point is mainly determined by the distance from the heat source. When the study point is far away from the heat source, the longer thermal equilibrium time is needed. Because the thermal equilibrium time of the spindle head is longer than that of the worktable. Therefore, the thermal equilibrium time of the machine tool is 56 hours. And the maximum thermal deformation of the machine tool is 224 μm in the direction of Z.

4.3 Experimental studies for model validation

4.3.1 Experimental conditions

To validate the proposed thermal analysis model, a long-time processing experiment was carried out on A2190 EDM machine tool shown in Fig. 11(a), keeping all the parameters same as the simulation settings. However, it is difficult to measure temperature rises of the electrode, workpiece and spindle head directly in real time when machining parts. Similarly, the thermal deformation of the spindle cannot be measured in real time.

In this work, the machine tool was therefore suspended after processing for every hour and the spindle head was raised to measure the temperature of the electrode. The temperature rise of the electrode surface was used as a reference to verify

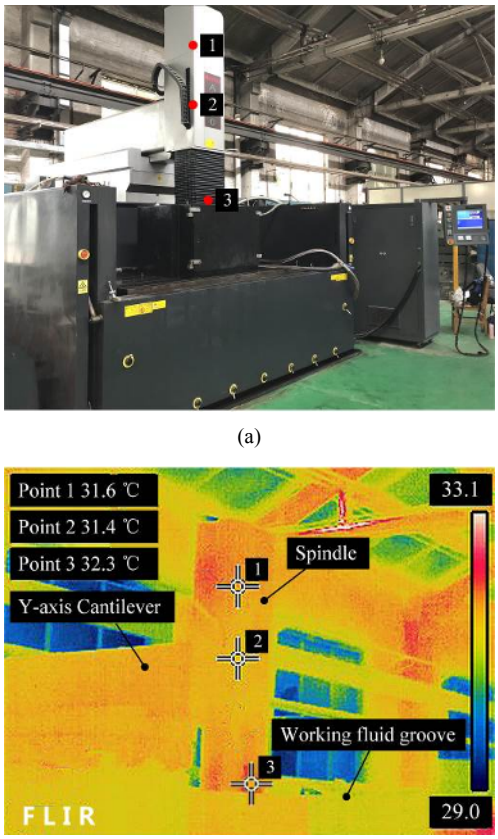

Fig. 11. The large-scale high-precision EDM machine tool (Model: A2190): (a) Experiment field; (b) thermal camera image of the spindle part and Y-axis cantilever.

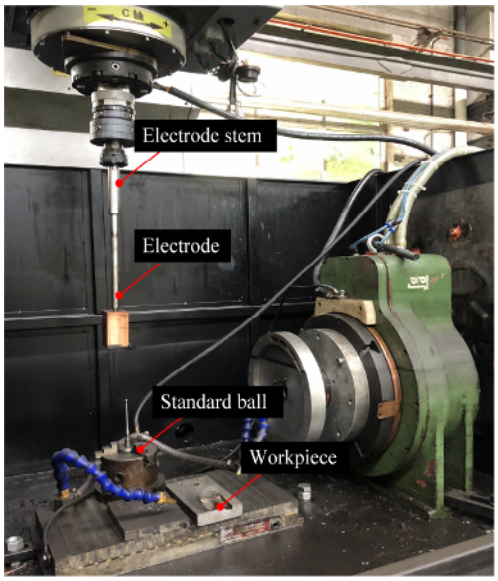

Fig. 12. The experimental setup.

the accuracy of simulation method. A thermal imaging camera (Model: FLIR T420) was set up to record temperature fields of machine structures. Fig. 12 shows the experimental setup.

A copper block with the similar discharge area of the simulated electrode was used to process the TC4. Note that the electrode was lifted off the liquid surface and photographed after processing for every hour, the test value may be different from the actual temperature during machining. The standard ball was applied to measure the displacement of the spindle head.

4.3.2 Experimental results

The temperature around the spindle structure (Z-axis column and base) and the Y-axis cantilever after running for 10 hours is shown in Fig. 11(b). The high temperature region was located at the upper and lower parts of the spindle. The temperature at spindle end (point 3) was about 0.9 K higher than other part of the spindle (point 2), which was in good agreement with the simulated result. In addition, some internal heat source of the spindle may cause the temperature rise at the upper part.

The temperature rise of each point on the electrode was extracted from the thermal images. Fig. 13 shows the thermal image of the electrode after processing for 1 hour. Obviously, the electrode showed the highest temperature rise (point 1 and 2) and the maximum was about 79.2 K, which demonstrated that the simulated and experimental results were comparable. The electrode stem material is stainless steel, whose thermal conductivity is 16.3 W/(m·K), much lower than copper, resulting in heat concentration. Hence, the temperature at the electrode top was the highest. The working fluid surface also showed a higher temperature (point 3).

In order to further assess the accuracy of the thermal simulation model, the simulated and measured value comparison diagram is shown in Fig. 14, where the same test point using in simulation. The equilibrium temperature in the experiment was about 21.4 K lower than that in the simulation, resulting in the error of 87 %. This may be caused by no continuous processing, leading to the slight decrease in temperature of the electrode whereby the heat accumulation on the electrode was difficult. In the simulation, the current value was taken as 200 A, which was the maximum machining current value given in the machine tool manual. In general, the actual output current of the power supply is usually lower than the value specified in the product manual. This is mainly due to the difference between test settings and operating conditions.

Moreover, after 6 hours of processing, the temperature of the test point has reached its steady state (95 % of its highest temperature rise), which is two hours late compared to the simulated results. The thermal equilibrium time depends on the maximum temperature rise and the time constant, which is determined by the specific heat capacity and the heat transfer coefficient. On one hand, the mechanical loss and hydraulic loss of the working fluid pump reduced the convective heat transfer coefficient. On the other hand, the recast layer thickness and micro cracks affected structure of the electrode surface would change the heat transfer coefficient, which was suspected to increase the thermal equilibrium time. Although the exact values of temperatures are not exactly the same, the order of the magnitude and general trend of the temperature change match very well.

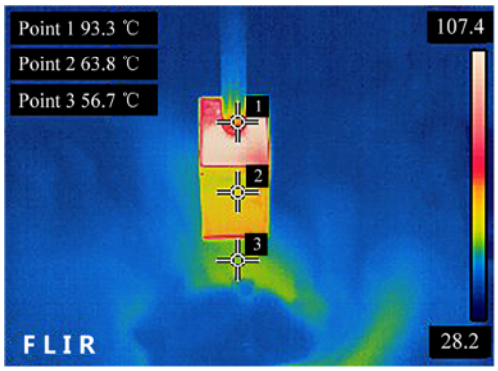

Fig. 13. Thermal image of the electrode after processing for 1 hour.

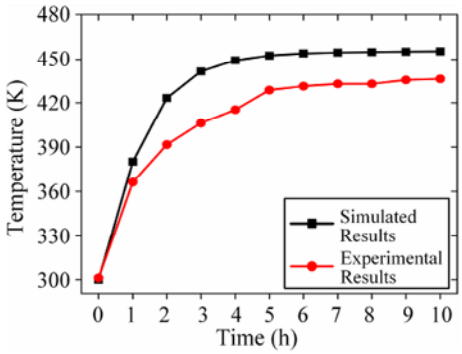

Fig. 14. The simulated and experimental results of the temperature of the electrode.

For the validation measurement of the displacement of the spindle, the standard ball were touched by the spindle before and after processing, and the Z-axis coordinates were recorded, which was the displacement of the spindle. The displacement was 0.08 mm along the negative direction of Z-axis and the error between numerical simulation and experiment was 7 %, suggesting that the theoretical result calculated by our model is close with the experimental result.

According to the results as mentioned above, the following suggestions for further improving the thermal stability and machining accuracy of large EDM machine tools are given:

(1) As the thermal equilibrium temperature of the working fluid is higher than the room temperature, the heat exchanger is needed to accelerate the heat dissipation of the tank, and hence the temperatures of fixed points can be turned down to control the temperature rise.

(2) The temperature sensor should be arranged on the spindle head. Based on the temperature measurement and the established thermal error model, the thermal error is obtained and then the position of the spindle can be adjusted to further improve the machining accuracy.

5. Conclusion

For the first time, a heat transfer model for predicting the thermal characteristics of a large precision EDM machine tool during long-time processing has been developed. The main conclusions can be drawn as follows:

(1) The equivalent heat flux, proved to be a valid alternative, is first proposed to model the intermittent heat flux on the machining surfaces for thermal analysis.

(2) Both the steady and transient analyses were applied to investigate the thermal equilibrium time of critical points. We found that when the study point is far away from the heat source, the longer thermal equilibrium time is needed. And the thermal equilibrium time of the machine tool was also estimated.

(3) The verification experiment was conducted. The temperature rise of the electrode surface was used as a reference to verify the accuracy of simulation method, indicating the simulation accuracy of 87 %. Although the exact values are not exactly the same, the order of the magnitude and general trend of the temperature change match very well.

(4) On the displacement of the spindle, the simulated result matched with the experimental result in Z direction error of 7 %.

Accordingly, the proposed thermal model with high accuracy, less complexity and low-cost satisfies the performance requirements of a fast identification system for thermal characteristics of large EDM machine tools.

Acknowledgments

This work is supported by National Natural Science Foundation of China (Grant No. 51775145), Major Project of Applied Technology Research and Development Plan of Heilongjiang Province (Grant No. GA16A404).

Nomenclature

Cp : Specific heat
h : Convection coefficient of working fluid
I : Peak current
k : Thermal conductivity
m : Instant of m
$\dot{Q}_{right}$: Heat flux flowing into the right surface
$\dot{Q}_{left}$: Heat flux flowing into the left surface
$\dot{Q}_{up}$: Heat flux flowing into the upper surface
$\dot{Q}_{bottom}$: Heat flux flowing into the bottom surface
$\dot{Q}_{front}$: Heat flux flowing into the right surface
$\dot{Q}_{back}$: Heat flux flowing into the back surface
$q(r)$: Heat flux density at the distance of r from the centre
$q_{eq}(r)$: Equivalent heat flux
r : Distance of r from the centre of the discharge
r_h : Spark radius
t_{on} : Discharge on-time
t_{off} : Pulse interval
$T_{x,y,z,m}$: Temperature of the element in X,Y,Z coordinates in instant m
Δt : Simulation time step
T_f : Ambient temperature of air or working fluid
U : Sustaining voltage of spark discharge
T_1 : Maximal temperature of the working fluid inside the groove
T_2 : Maximal temperature of the working fluid inside the tank
T_3 : Maximal temperature of the selected point on the electrode
T_4 : Maximal temperature of the selected point on the workpiece
T_5 : Maximum temperature of the worktable surface
T_6 : Average temperature of the bottom of the spindle head

Greek symbols

η : Effectiveness
ρ : Mass density

References

[1] A. M. Abdulshahed, A. P. Longstaff, S. Fletcher and A. Myers, Thermal error modelling of machine tools based on ANFIS with fuzzy c-means clustering using a thermal imaging camera, *Applied Mathematical Modelling*, 39 (2015) 1837-1852.

[2] J. Zhang, P. Feng, C. Chen, D. Yu and Z. Wu, A method for thermal performance modelling and simulation of machine tools, *International Journal of Advanced Manufacturing Technology*, 68 (2013) 1517-1527.

[3] S. H. Wankhade and S. B. Sharma, Study of the productivity and surface quality of hybrid EDM, *Journal of the Institution of Engineers*, 97 (1) (2015) 1-6.

[4] S. Kumar, Status of recent developments and research issues of electrical discharge machining (EDM), *International Journal of Latest Trends in Engineering and Technology*, 2 (3) (2013) 242-248.

[5] I. Ayesta, B. Izquierdo, J. A. Sanchez, J. M. Ramos, S. Plaza, I. Pombo and N. Ortega, Optimum electrode path generation for EDM manufacturing of aerospace components, *Robotics and Computer-Integrated Manufacturing*, 37 (2016) 273-281.

[6] A. Ahmed, A. Fardin, M. Tanjilul, Y. S. Wong and M. A. Senthil Kumar, A comparative study on the modelling of EDM and hybrid electrical discharge and arc machining considering latent heat and temperature-dependent properties of Inconel 718, *International Journal of Advanced Manufacturing Technology*, 1 (2017) 1-9.

[7] Y. Zhao, M. Kunieda and K. Abe, EDM mechanism of single crystal SiC with respect to thermal, mechanical and chemical aspects, *Journal of Materials Processing Technology*, 236 (2016) 138-147.

[8] T. Wang, J. Zhe, Y. Q. Zhang, Y. L. Li and X. R. Wen,

Thermal and fluid field simulation of single pulse discharge in dry EDM, *The Seventeenth CIRP Conference on Electro Physical and Chemical Machining*, 6 (2013) 427-431.

[9] Y. Zhang, Y. Liu, Y. Shen, Z. Li, R. Ji and B. Cai, A novel method of determining energy distribution and plasma diameter of EDM, *International Journal of Heat & Mass Transfer*, 75 (8) (2014) 425-432.

[10] Y. Shen, J. Chen, Y. Yang, K. Zhang, Y. Li and B. Zhu, Study on the characteristics of plasma channel based on multi-spark pulse discharge machining effect, *International Journal of Advanced Manufacturing Technology*, 97 (5-8) (2018) 1-8.

[11] K. P. Somashekhar, S. Panda, J. Mathew and N. Ramachandran, Numerical simulation of micro-EDM model with multi-spark, *International Journal of Advanced Manufacturing Technology*, 76 (2015) 83-90.

[12] A. Varghese, B. Kuriachen, S. Panda and J. Mathew, Experiments and simulation of three dimensional micro EDM with single and multiple discharges, *All India Manufacturing Technology, Design and Research Conference* (2014) 3271-3276.

[13] F. Klocke, S. Schneider, M. Mohammadnejad, L. Hensgen and A. Klink, Inverse simulation of heat source in electrical discharge machining (EDM), *Procedia Cirp*, 58 (2017) 1-6.

[14] N. S. Mian, S. Fletcher, A. P. Longstaff and A. Myers, Efficient thermal error prediction in a machine tool using finite element analysis, *Measurement Science & Technology*, 22 (8) (2011) 085107.

[15] E. Gomez-Acedo, A. Olarra, J. Orive and L. N. L. D. L. Calle, Methodology for the design of a thermal distortion compensation for large machine tools based in state-space representation with Kalman filter, *International Journal of Machine Tools & Manufacture*, 75 (2013) 100-108.

[16] B. Kuriachen, A. Varghese, K. P. Somashekhar, S. Panda and J. Mathew, Three-dimensional numerical simulation of microelectric discharge machining of Ti-6Al-4V, *International Journal of Advanced Manufacturing Technology*, 79 (1-4) (2015) 147-160.

[17] M. A. Singh, K. Das and D. K. Sarma, Thermal simulation of machining of alumina with wire electrical discharge machining process using assisting electrode, *Journal of Mechanical Science & Technology*, 32 (1) (2018) 333-343.

[18] B. Izquierdo, J. A. Sánchez, N. Ortega, S. Plaza and I. Pombo, Insight into fundamental aspects of the EDM process using multidischarge numerical simulation, *International Journal of Advanced Manufacturing Technology*, 52 (2011) 195-206.

[19] S. N. Joshi and S. S. Pande, Thermo-physical modelling of die-sinking EDM process, *Journal of Manufacturing Processes*, 12 (2010) 45-56.

[20] H. Singh, Experimental study of distribution of energy during EDM process for utilization in thermal models, *International Journal of Heat and Mass Transfer*, 55 (2012) 5053-5064.

[21] A. Al-Khazraji, S. A. Amin and S. M. Ali, The effect of SiC powder mixing electrical discharge machining on white layer thickness, heat flux and fatigue life of AISI D2 die steel, *Engineering Science & Technology an International Journal*, 19 (3) (2016) 1400-1415.

[22] C. Xia, J. Fu and Y. Xu, Machine tool selected point temperature rise identification based on operational thermal modal analysis, *International Journal of Advanced Manufacturing Technology*, 70 (2014) 19-31.

Zhaoxi Zhao is a Ph.D. student in the School of Mechatronics Engineering of Harbin Institute of Technology and a member in Key Laboratory of Microsystems and Micro-structures Manufacturing of Ministry of Education at the same institute. Her research work focuses on the dynamic and thermal analysis of large precision die-sinking EDM machine tools.

Zhenlong Wang is a Professor and an Associate Dean in the School of Mechatronics Engineering of Harbin Institute of Technology. His research area is on non-traditional machining technology, micro-machining technology, electro-mechanical control process and intelligent processing. In recent years, he has completed more than 30 projects including the key projects of the National Natural Science Foundation and the National 863 Program, the advance research projects of the General Equipment Department, the basic scientific research projects of the National Defense Science and Industry Commission, and 973 projects.